Journal of Molecular Liquids 398 (2024) 124270

Contents lists available at ScienceDirect

Journal of Molecular Liquids

journal homepage: www.elsevier.com/locate/molliq

Template assisted hydrothermal synthesis of bismuth vanadate for Rhodamine B photodegradation

Said Essenni [a], Moonis Ali Khan [b,*], Rachid El kaim billah [c], Byong-Hun Jeon [d], Suresh Sundaramurthy [e], Mahfoud Agunaou [a]

[a] Laboratory of Coordination and Analytical Chemistry (LCCA), Faculty of Science, Chouaib Doukkali University (UCD), 24000 El Jadida, Morocco
[b] Chemistry Department, College of Science, King Saud University, Riyadh 11451, Saudi Arabia
[c] Science Engineer Laboratory for Energy, National School of Applied Sciences, Chouaib Doukkali University, El Jadida, Morocco
[d] Department of Earth Resources and Environmental Engineering, Hanyang University, Seoul 04763, South Korea
[e] Department of Chemical Engineering, Maulana Azad National Institute of Technology, Bhopal 462 003, M.P., India

ARTICLE INFO

Keywords:
Biopolymer
Chitosan
Surfactants
Pluronic 123
Photocatalysis
Organic dye

ABSTRACT

Developmental and technological activities result in uncontrollable release of synthetic dyes into water reservoirs posing potential threat to flora and fauna. Thus, the development of suitable process to treat these waste effluents is urgently needed. Herein, a facile technique was employed to synthesize bismuth vanadate ($BiVO_4$) by incorporating Chitosan (Cs) and Triblock pluronic 123 (P) as directing agents through the hydrothermal process and its efficacy as a photocatalyst was tested for Rhodamine B (RhB) photodegradation. It is noteworthy that the use of Cs as template during the synthesis of $BiVO_4$ had not been previously documented. The synthesized materials were subject to a comprehensive array of characterization techniques, including XRD, FTIR, UV–visible diffuse reflection, SEM, TEM, N_2 adsorption isotherm, and XPS analyses. The outcomes revealed that the synthesized catalysts have a monoclinic scheelite structure and displayed an irregular morphology. In addition, the particle size decreased remarkably with the use of Cs. The XPS revealed that the templates have a major influence on the surface charge of the material, as revealed by point of zero charge (pH_{PZC}) analysis. Notably, $BiVO_4$-Cs exhibited the highest specific surface area (SSA: 12.27 m^2/g) among them. The synthesized photocatalysts exhibited high catalytic stability. Additionally, the photocatalysts showed excellent RhB photodegradation performance of 94.2 and 64.4 % under UV-B and visible light illumination, respectively.

1. Introduction

In recent years, the photocatalytic process has received considerable attention for its capacity to efficiently transform hazardous organic pollutants into ecologically benign compounds at room temperature. This approach has been widely studied to reduce the presence of various toxic organic pollutants by completely mineralizing them [1–4]. The photocatalytic treatment of contaminated water has been achieved using various photocatalysts, including TiO_2, Bi_2O_3, and ZnO [5–7]. Among the photocatalysts used during heterogeneous photocatalysis, bismuth vanadate ($BiVO_4$) occupies a prominent position. It has attracted considerable interest because of its exceptional physicochemical properties including a narrow energy band, a marked rise in potential at the valence band position, a lack of toxicity, and a remarkable stability [8,9]. According to previous reports, $BiVO_4$ can be found in three different crystal structures: the monoclinic scheelite, the tetragonal scheelite, and the tetragonal zircon [10,11]. $BiVO_4$ with tetragonal structure, having 3.11 eV band gap absorbs ultraviolet (UV) rays, while $BiVO_4$ with a monoclinic scheelite structure (with 2.34 eV band gap) absorbs both visible and UV radiations [12].

Aqueous [13–15], hydrothermal [9,16–18], sonochemical [19,20], and solid-state reaction [21] methodologies have been well reported to synthesize $BiVO_4$ crystallites with a monoclinic structure. In recent years, trend has been set on using a wide range of surfactant and directing agents based organic templates such as cetyltrimethylammonium bromide (CTAB) [22], sodium carboxymethylcellulose (SCMC) [23], and ethylenediamine tetra acetic acid (EDTA) [24] to synthesize crystals with specific morphologies and impeccable structures. Triblock Pluronic 123 (P) has found extensive application as a template in numerous research endeavors focused on $BiVO_4$. Meng et

* Corresponding author.
E-mail address: mokhan@ksu.ed.sa (M. Ali Khan).

https://doi.org/10.1016/j.molliq.2024.124270
Received 13 December 2023; Received in revised form 1 February 2024; Accepted 13 February 2024
Available online 23 February 2024

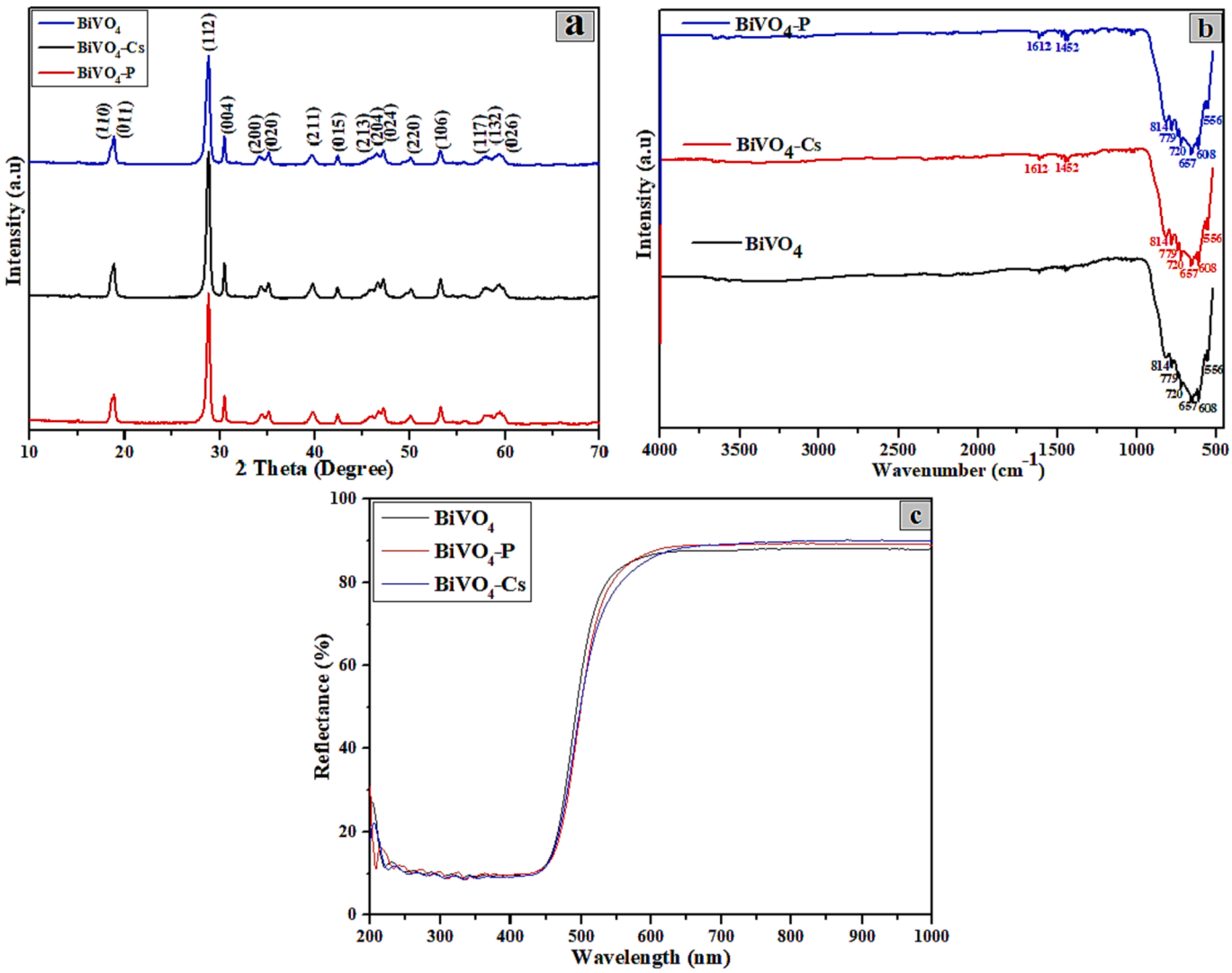

Fig. 1. X-ray diffraction patterns (a), FT-IR spectra (b), UV–vis diffuse reflectance spectra (c) of the samples.

al [25] synthesized monoclinic $BiVO_4$ single crystals with varying shapes using a surfactant-assisted hydrothermal method and successfully tested their capability to photocatalytically degrade methylene blue (MB) under visible light. Jiang et al [26] synthesized monoclinic $BiVO_4$ single crystals with polyhedral, spherical, or octapod-like porous structures using the triblock copolymer P-assisted hydrothermal method and evaluated its photocatalytic efficiency in removing MB and phenol upon exposure to visible light. In another study, $BiVO_4$ with different morphologies were synthesized by surfactant-assisted microwave methodology and decorated with CdS through chemical-bath-deposition method ($BiVO_4$-CdS). Hollow structure $BiVO_4$-CdS (synthesized using EDTA as template material) displayed highest photodegradation performances for tetracycline hydrocholoride and ciprofloxacin[27]. As far as we are aware, there is no existing information regarding the utilization of the biopolymer chitosan (Cs) as a directing agent in the synthesis of $BiVO_4$.

Thus, the current research was aimed on examining, for the first time, the impact of Cs compared it with P as template materials on the optical and morphological characteristics of hydrothermally synthesized $BiVO_4$. Furthermore, the photocatalytic efficiency of hydrothermally synthesized $BiVO_4$ has been evaluated. The morphological, optical, chemical, and surface characteristics of $BiVO_4$ were tested through XRD, FTIR, UV/Vis scattering reflectance spectroscopy, SEM, TEM, N_2 adsorption/desorption, and XPS analyses. Rhodamine B (RhB) photodegradation under UV-B and visible light irradiations were tested to assess the photocatalytic efficacy of synthesized materials.

2. Materials and methods

2.1. Chemicals and reagents

Analytical reagent (A.R) grade chemicals were used during the research or as itemized. Ammonium metavanadate (NH_4VO_3, ≥99.5 %), ammonium hydroxide solution (NH_4OH, ≥32 %), and bismuth nitrate pentahydrate ($Bi(NO_3)_3{\cdot}5H_2O$, ≥98 %) were purchased from Sigma-Aldrich, USA. Nitric acid (HNO_3), acetic acid (CH_3COOH), and ethanol (C_2H_5OH) were purchased from Sigma-Aldrich, Germany. Triblock Pluronic 123 (P), chitosan (Cs), isopropanol, ethylenediaminetetraacetic acid (EDTA), and sodium carbonate (Na_2CO_3) were purchased from Merck, Germany. The target pollutant RhB was procured from Laboratories SOLVACHIM.

2.2. Synthesis of $BiVO_4$

$BiVO_4$ was synthesized through hydrothermal method using templates. During the synthesis, 0.585 g NH_4VO_3, under continuous stirring at 70 °C, was solubilized in 30 mL deionized (DI) water. Simultaneously, 2.425 g of $Bi(NO_3)_3{\cdot}5H_2O$ was dissolved in 10 mL concentrated HNO_3.

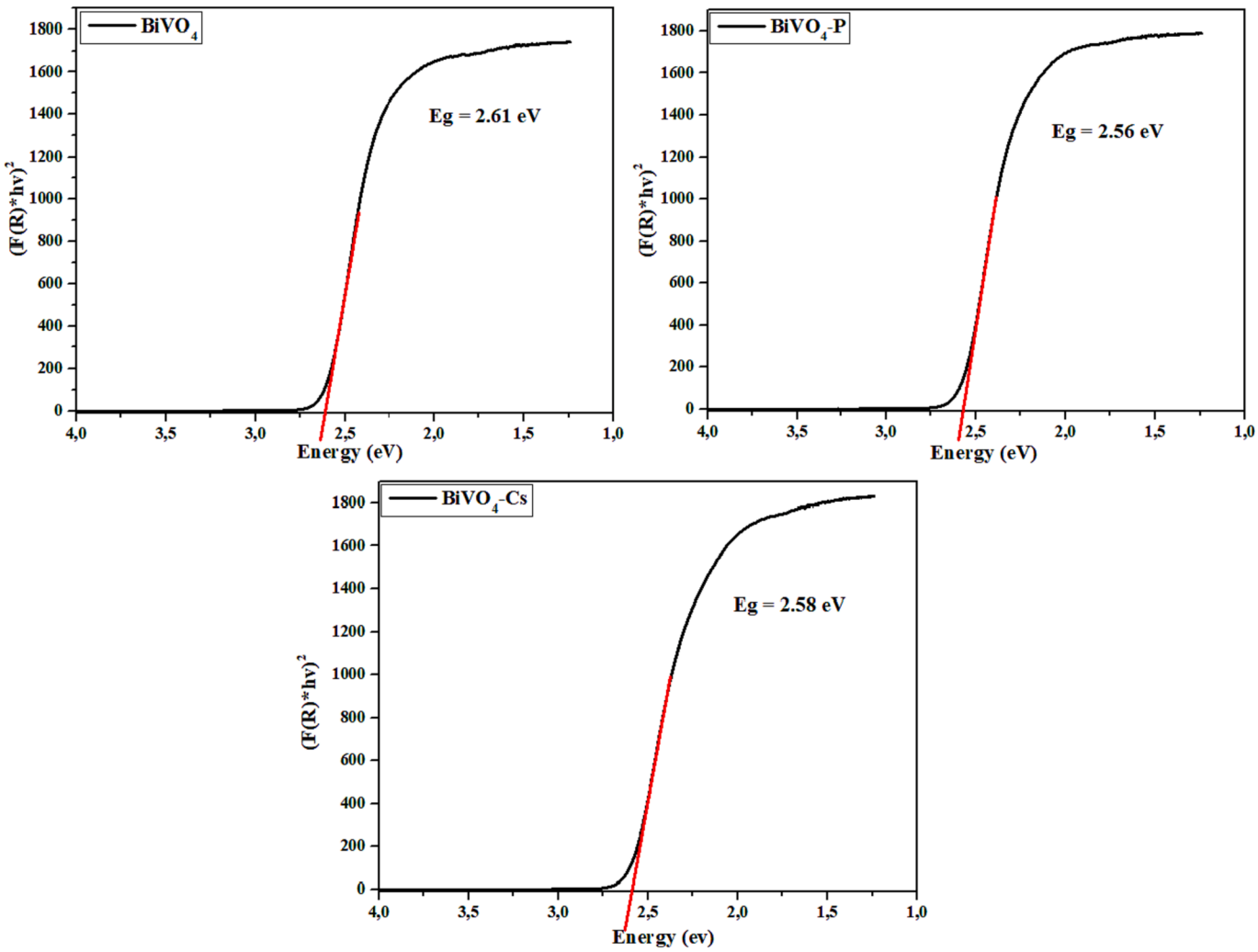

Fig. 2. Plots of $(F(R)*h\upsilon)^2$ versus photon energy ($h\upsilon$).

Both solutions were mixed under continuous stirring. Subsequently, one of the templates (Cs in 10 mL 1 % CH_3COOH or P in 10 mL DI water) was gradually introduced into the mixture. The stirring continued for an hour, while the pH was adjusted to 9 by adding a 32 % NH_4OH solution. The mixture was then transferred to Teflon lined autoclaved (with 100 mL capacity) and was treated at 100 °C for 2 h. Finally, the synthesized solid product was filtered, washed (with DI water and ethanol), dried overnight at 120 °C, and calcined at 450 °C for 3 h in a tubular furnace. The synthesized materials were labeled as $BiVO_4$ (without any template), $BiVO_4$-P (using triblock Pluronic 123 as template), and $BiVO_4$-Cs (using chitosan as template).

2.3. Characterization of $BiVO_4$

The crystal structures of the $BiVO_4$ photocatalysts were analyzed using a BRUKER-binary V2, model D8 diffractometer with Cu Kα radiation (λkα = 1.5418 Å). The samples were scanned between 2θ = 5.00° and 69.98° with a 0.02° step. Fourier transform infrared (FTIR) spectra in the range of 400–4500 cm^{-1} were obtained using a Nicolet iS10 Thermo Fisher FTIR spectrometer. Perkin-Elmer Lambda 365 UV/Vis spectrophotometer was used to record Diffuse reflectance UV–vis spectra. The morphologies and elemental compositions of synthesized photocatalysts were studied by high resolution scanning electron microscopy coupled with energy dispersive X-ray (HRSEM-EDX), low vacuum SEM (LV-SEM) (S-3500 N, Hitachi) and transmission electron microscopy (TEM), Leo 912A 8B OMEGA EF-TEM (Carl Zeiss, Germany), Surface elemental and chemical states were observed by X-ray photoelectron spectroscopy (XPS) using a theta probe-based system (Thermo Fisher Scientific). BET surface area was measured using 3Flex (Micromeritics, USA).

2.4. Photocatalysis study

The photocatalytic efficiency of $BiVO_4$ sample was evaluated by studying the photocatalytic degradation of RhB under UV-B and visible radiations. This assessment was conducted in a reactor utilizing either six low-pressure lamps (TL29D16/09 N; 105 W; Philips model) emitting UV-B radiation or three halogen lamps (F15T8/D; 15 W) emitting daylight, all operated at room temperature. A beaker (100 mL) was selected as a reaction vessel. The distance between the lamps and the solution was 12 cm. The photodegradation experiments were conducted under ambient temperature conditions. $BiVO_4$ sample (amount, m: 25 – 75 mg) was suspended in 50 mL of RhB solution (initial concentration, C_o: 5 – 15 mg/L), and pH (4, 7, and 8). Before exposure to irradiation, the suspension was stirred continuously for 30 min in darkness to establish adsorption/desorption equilibrium between $BiVO_4$ sample and RhB solution. At specified intervals, one milliliter aliquot of RhB solution was extracted from the suspension. The aliquot was passed through a 0.45 μm pore filter to ensure complete removal of photocatalyst sample. The absorbance was measured at the maximum absorption wavelength (λ_{max}: 554 nm) using a UV–Vis spectrophotometer (V-1100 D spectrophotometer). Photocatalytic degradation efficiency (R, %) was

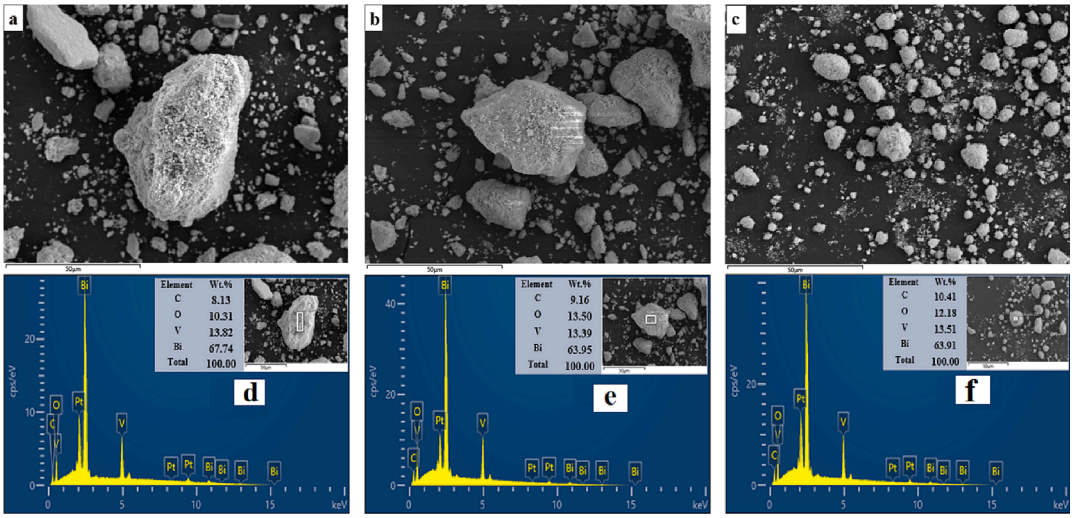

Fig. 3. SEM images of $BiVO_4$ (a), $BiVO_4$-P (b), $BiVO_4$-Cs (c), EDX spectrum of $BiVO_4$ (d), $BiVO_4$-P (e), and $BiVO_4$-CS (f) (Inset: elemental analysis data).

assessed as follows:

$$R, \% = \frac{(C_o - C_t)}{C_o} \times 100 \quad (1)$$

Where C_o and C_t are RhB concentrations before illumination and at t irradiation time, respectively.

3. Results and discussion

3.1. Photocatalysts samples characterization

Fig. 1**a** displayed the XRD pattern of $BiVO_4$ samples. The diffraction peaks observed in the photocatalyst samples were associated with a monoclinic scheelite structure (JCPDS No. 01–083-1699), consistent with previous works [17,28]. No diffraction signals from other crystalline impurities were observed. The crystallite sizes (D_{XRD}, nm) of $BiVO_4$, $BiVO_4$-P, and $BiVO_4$-Cs crystals calculated by Scherrer's equation were 21, 15, and 13 nm, respectively. A significant decrease D_{XRD} was observed with the use of template during the synthesis. In addition, the intensities of the distinctive peaks associated with $BiVO_4$ showed variable alterations after the incorporation of directing agents. As shown in Fig. 1**a**, the relative intensity ratios calculated for facets (1 1 2) and (0 0 4) were 4.6 for $BiVO_4$, 3.8 for $BiVO_4$-P, and 3.7 for $BiVO_4$-Cs. These results suggest certain influence of the two directing agents on the crystal structure of the oxide.

The chemical functionalities present on synthesized photocatalysts surface were studied through FTIR analysis, and the spectra are shown in Fig. 1**b**. Two peaks at 556 and 608 cm^{-1}, ascribed to the Bi-O vibration were observed [29]. In addition, two peaks at 657 and 779 cm^{-1} corresponding to VO_4^{3-} vibrations were observed [29]. A peak associated with the asymmetric stretching of VO_4^{3-} was observed at 720 cm^{-1} [30]. The V-O vibration peak appeared at 814 cm^{-1} [31]. The absorption band at 1452 cm^{-1} could be assigned to C–OH vibration [32]. Additionally, a faint band at 1612 cm^{-1} was associated with H-O–H stretching [33].

The UV–vis spectrophotometer was employed to measure the optical absorption spectra of $BiVO_4$ samples. In Fig. 1**c**, the UV–vis diffuse reflectance spectra are presented. The absorption edges of the synthesized monoclinic materials were observed at approximately 450 nm. In the context of a semiconductor, the optical absorption near the band edge is expressed as follows [34]:

$$\alpha h\upsilon = A\,(h\upsilon - E_g)^{n/2} \quad (2)$$

where α, ν, E_g, and A are the absorption coefficient, light frequency, band gap, and a constant, respectively. Notably, the parameter n is contingent upon the transition characteristics in a semiconductor, specifically, whether it is a direct (n = 1) or indirect (n = 4) transition. In the case of $BiVO_4$, the value of n is determined to be 1 [35].

For the powder sample, the optical band gap was calculated using diffuse reflectance spectroscopy (DRS) employing the Kubelka-Munk method. Throughout this investigation, the absorption coefficient was substituted with the Kubelka-Munk function F(R), expressed as:

$$F(R) = \frac{(1-R)^2}{2R} \quad (3)$$

where R represents the reflectance of the material, the band gap energy values are ascertained through the extrapolation of the linear portion of the curve $(F(R)*h\nu)^2$ vs hν to the energy axis. The point of intercept on the energy axis (hν) at which $(F(R)*h\nu)^2 = 0$ serves as the indicator for the band gap value. The calculated optical band gaps for $BiVO_4$, $BiVO_4$-P and $BiVO_4$-Cs were 2.61, 2.56 and 2.58 eV, respectively, illustrated in Fig. 2 **(a – c)**.

SEM images illustrates the hydrothermally fabricated $BiVO_4$, $BiVO_4$-P, and $BiVO_4$-Cs (Fig. 3 **(a – c)**). It was evident that the particle sizes of these oxides were primarily influenced by the choice of template used. In terms of morphology, all samples exhibited irregularly shaped particles and small agglomerations with different size, underscoring the influence of directing agents on the particle size. When synthesizing $BiVO_4$ without any additives, the resulting particles were characterized by large irregular forms, measuring 32 μm in length. The use of P as a template ($BiVO_4$-P) had a minimal effect on particle size, resulting in particles with a length of 30 μm. In contrast, the introduction of Cs had a substantial impact on the morphology, notably reducing particle size to 11 μm in length.

The photocatalytic efficacy of the synthesized materials is notably influenced by the structural characteristics of the particles. Generally, surfactants exert a significant influence on synthesizing photocatalysts with high specific surface area (SSA) and small particle morphology. Fan et al. [36] synthesized $BiVO_4$ crystals with varying morphologies using a hydrothermal method, by adjusting the quantity of introduced surfactant. Notably, a sample with a flower-like morphology exhibited superior photocatalytic activity, primarily due to its expanded SSA and enhanced efficiency in separating photo-induced charge carriers. Similarly, Zeng et al. [37] outlined the synthesis of $BiVO_4$ microcrystals through a surfactant assisted hydrothermal method, while polling a range of parameters related to SSA, structure, morphology, and photo-induced charge separation efficiency (PCSE). Incorporation of surfactant, sodium dodecylbenzenesulfonate (SDBS) raised PCSE of $BiVO_4$ when exposed to solar radiations. This results a remarkable 7.5-fold rise

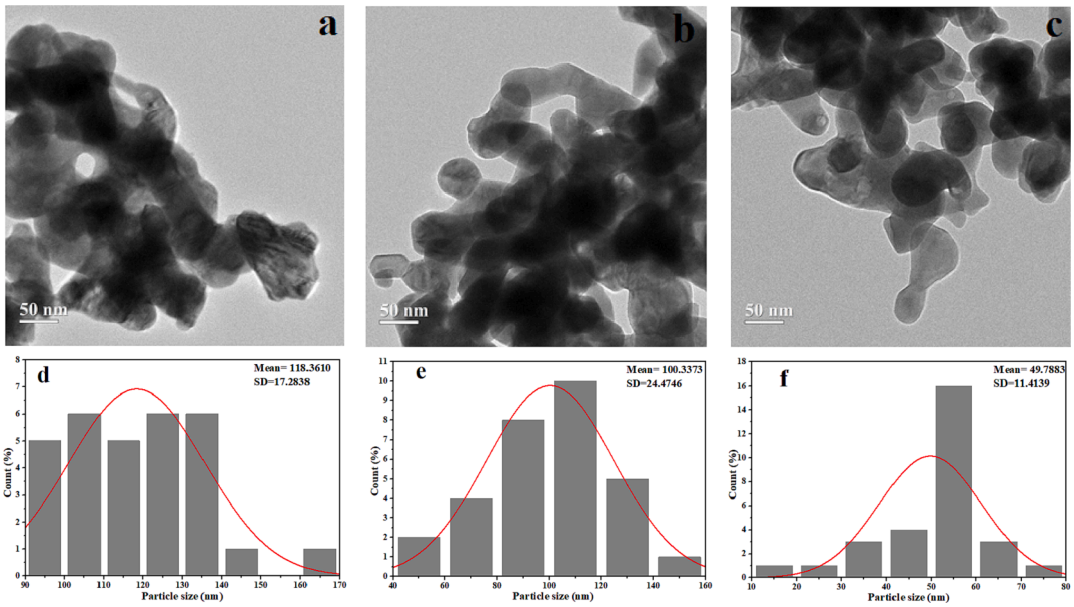

Fig. 4. TEM images of $BiVO_4$ (a), $BiVO_4$-P (b), $BiVO_4$-Cs (c), particle size distribution plots of $BiVO_4$ (d), $BiVO_4$-P (e), and $BiVO_4$-Cs (f) fitted with a log normal distribution function.

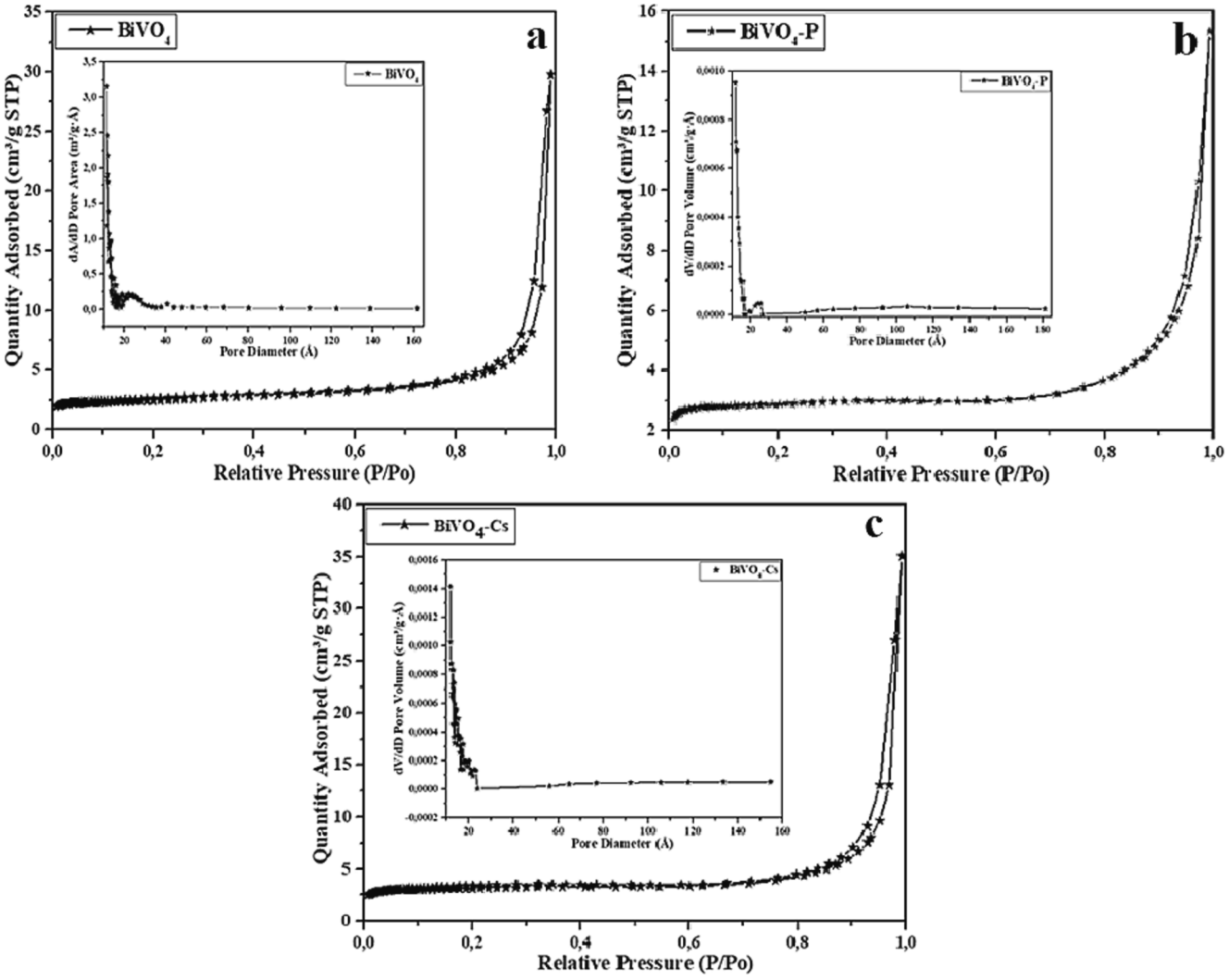

Fig. 5. N_2 adsorption/desorption plots of $BiVO_4$ (a), $BiVO_4$-P (b), and $BiVO_4$-Cs (c) samples (Inset: pore size distribution plots).

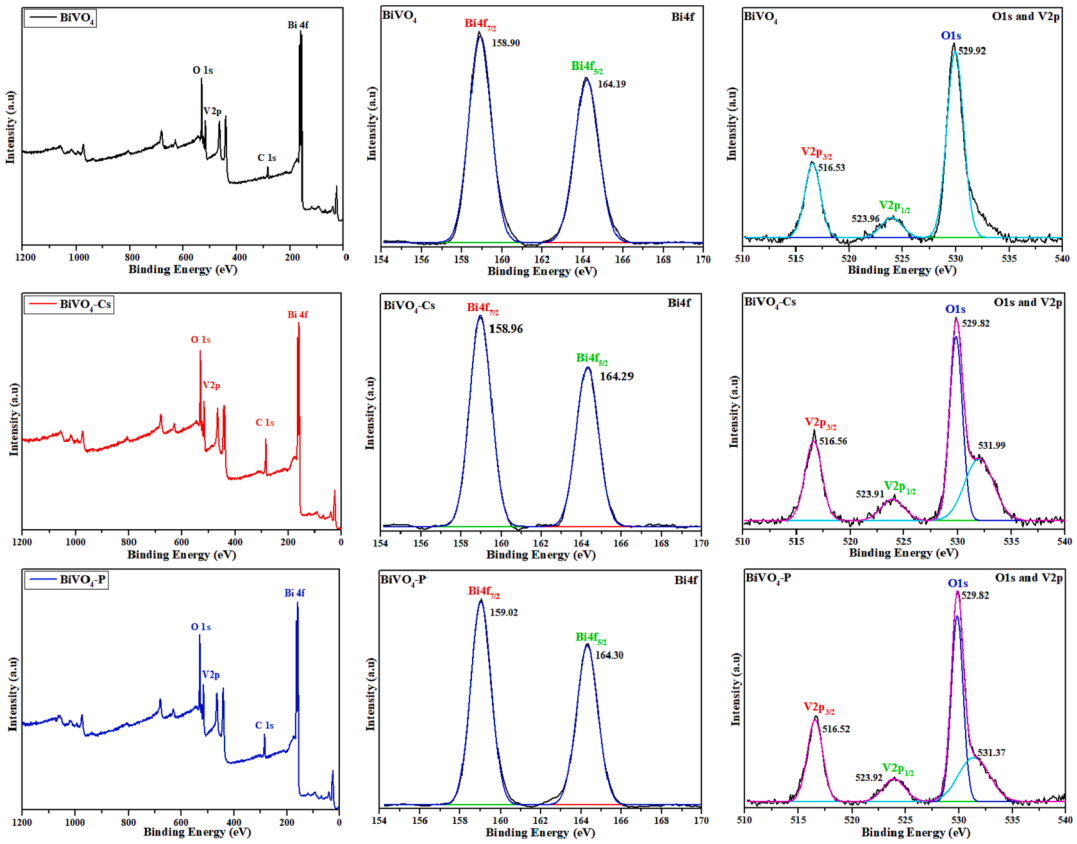

Fig. 6. Overall survey and deconvoluted XPS spectra of the samples.

in RhB photocatalytic degradation. Liu et al. [38] explored the impact of templates on both morphology and photocatalytic activity of the synthesized oxides. The results revealed that the oxide prepared with SDBS as template exhibited an irregular flake-like morphology and high SSA, resulting in the highest observed photocatalytic activity.

The EDX spectrum validates the elemental makeup of the material. The spectra distinctly reveal the existence of bismuth (Bi), vanadium (V), oxygen (O), and carbon (C), while the platinum (Pt) signal was derived from the sputtered Pt nanoparticles employed in the SEM analysis, as depicted in Fig. 3 **(d – f)**. The most obvious interpretation suggests that the compound was $BiVO_4$, given the great similarity in the distribution of Bi, V and O, and the C signal suggests surface carbon adsorption in case of $BiVO_4$ or the presence of directing agents in the instances of $BiVO_4$-P and $BiVO_4$-Cs.

As shown in Fig. 4 **(a - c)**, the presence of directing agents had a positive effect on the particle size of the synthesized oxides. In addition, the images revealed that the materials obtained were in nanoparticles size range and exhibited an irregular morphology.

A log-normal distribution is fitted to the particle size distribution histogram to estimate the average particle size for each sample [39].

$$f(D) = \left(\frac{1}{\sqrt{2\pi}\,\sigma_D}\right) e^{\left[-\frac{ln^2\left(\frac{D}{D_0}\right)}{2\sigma^2}\right]} \quad (4)$$

where D represents the average particle size, and σ_D denotes the standard deviation. The fitting of the log-normal distribution function to the particle size distribution histogram for the prepared samples is exemplified in Fig. 4 **(d – f)**. The calculated D for $BiVO_4$, $BiVO_4$-P, and $BiVO_4$-Cs were found to be 118, 100, and 80 nm along with σ_D of 17.28, 24.47 and 18.24 nm, respectively. The observed D values were found to decrease with directing agent.

The synthesized samples were subjected to the evaluation of their surface textural characteristics using the N_2 absorption–desorption curves (Fig. 5 **(a – c)**). The adsorption/desorption isotherms of all the oxides exposed an H3-type loops with a type-IV hysteresis curves. This affirmed mesoporosity among the synthesized samples. Through this analysis, the Brunauer Emmett Teller (BET) method was used to calculate the SSA and the Barret Joyner Halender (BJH) method was used to determine the pores size. The SSA for $BiVO_4$, $BiVO_4$-P, and $BiVO_4$-Cs were 9.20, 11.60, and 12.27 m^2/g, respectively. In addition, the calculated average pore volume as well as the pore diameter were 0.0082 cm^3/g and 3.86 nm for $BiVO_4$, 0.0061 cm^3/g and 3.29 nm for $BiVO_4$-P, and 0.0089 cm^3 /g and 2.93 nm for $BiVO_4$-Cs. The largest SSA was observed for $BiVO_4$-Cs, could be associated with an increase in its photocatalytic activity [40–42].

In addition, the overall XPS analysis survey results confirmed the presence of C, Bi, O, and V in the samples, illustrated in Fig. 6. The deconvoluted XPS spectra for the samples displayed two distinct peaks for Bi 4f corresponding to Bi $4f_{7/2}$ and Bi $4f_{5/2}$. Similarly, the V 2p spectra corresponds to V $2p_{3/2}$ and V $2p_{1/2}$, indicating the existence of a V^{5+} state in $BiVO_4$ structures. Notably, the O1s XPS spectrum for the oxide synthesized without any directing agent shows a single peak at 529.92 eV. In contrast, the XPS spectra of $BiVO_4$-P and $BiVO_4$-Cs showed asymmetric oxygen state behavior, with deconvoluted peaks centered at around 529.82 and 531.99 eV, attributed to the lattice oxygen and surface hydroxyl groups of $BiVO_4$, respectively [43–47].

3.2. Photocatalytic application

3.2.1. Effect of pH on RhB photodegradation

Impact of pH conditions on photocatalytic degradation rates is complex, and the effect observed generally depends on the specific type of pollutant and the point of zero charge (pH_{pzc}) of the semiconductor

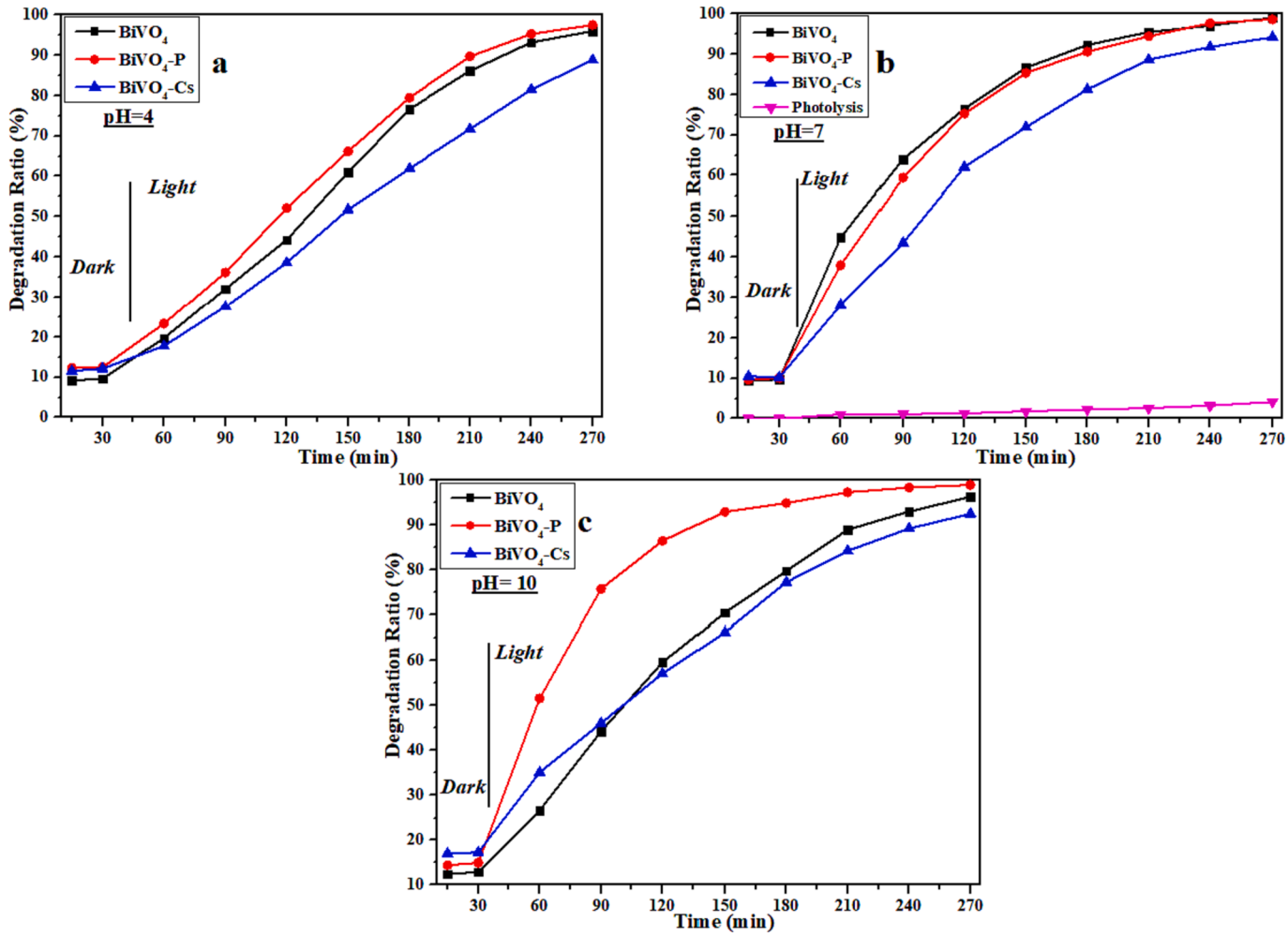

Fig. 7. Effect of pH 4 (a), pH 7 (b), and pH 10 (c) on RhB degradation rate.

used during photodegradation [48,49]. The determination of pH_{pzc} of $BiVO_4$ was carried out following the methodology outlined by Khalaf et al [50] and results presented in **Fig. S1** suggest that the materials synthesized using directing agents consistently have a negative surface charge. In contrast, the observed pH_{pzc} for $BiVO_4$ was 7.48, indicating that the surface assumes a negative charge for pH values exceeding the pH_{pzc} and a positive charge for pH values below it. The results of this study indicate that the guiding agents have a perceptible impact on the surface charge of the synthesized samples. This phenomenon might account for the modification of the surface charge induced by the presence of hydroxyl groups on the surface of these materials, a confirmation established through XPS analysis.

To assess the impact of UV-B light on RhB degradation in the absence of a catalyst, a preliminary experiment involving the direct photolysis of RhB (blank experiment) under identical conditions was conducted. This experiment revealed that RhB did not undergo photolysis under UV-B light irradiation. Thereafter, to assess the influence of pH on RhB photodegradation efficiency, pH was adjusted to 4, 7 and 10, prior to reaction by adding NaOH or HCl (0.1 mol/L) to the solution under the following conditions (RhB C_o: 5 mg/L and m: 50 mg) (Fig. 7 **a – c**). The results presented in Fig. 7**b** highlights the effectiveness of RhB reduction by $BiVO_4$ in a neutral environment, while $BiVO_4$-P showed slightly better RhB reduction in acidic and basic mediums than in neutral medium, illustrated in Fig. 7**a and c**. However, the overall RhB reduction performances by $BiVO_4$, $BiVO_4$-P, and $BiVO_4$-Cs under neutral pH conditions were efficient and almost nearer. Consequently, the optimum pH value determined in this research was 7.

3.2.2. *Effect of catalyst dose*

The RhB photocatalytic degradation involved varying catalyst dose (m) within the range of 25 to 75 mg/L. A marginal yet noteworthy enhancement in degradation was observed with an increase in m from 25 to 75 mg/L, depicted in Fig. 8 **a - c**. This phenomenon was attributed to the increased availability of active sites on the catalyst surface and improved penetration of UV-B light into the suspension, leading to an augmentation of total active surface sites with higher catalyst dosage. However, at m > 50 mg/L, a decrease in UV-B light penetration due to the shielding effect caused by an excess of catalyst particles in the solution was noted [51]. Consequently, the optimal catalyst sample amount for RhB photocatalytic degradation was determined to be 50 mg/L. Nonetheless, $BiVO_4$ and $BiVO_4$-Cs exhibited a slight improvement in the photodegradation rate when the catalyst amount was increased to 75 mg/L.

3.2.3. *Effect of dye concentration*

The RhB photocatalytic degradation was also investigated at various initial concentrations (C_o: 5 to 15 mg/L). The initial rate of RhB photodegradation exhibited a declining trend with increasing concentration, as illustrated in Fig. 9 **a - c**. This behavior can be elucidated by recognizing that with elevated initial concentrations, more RhB molecules were adsorbed onto the $BiVO_4$ surface. This, in turn, diminishes the production of hydroxyl radicals, as there are fewer active sites available for hydroxyl ion adsorption and subsequent hydroxyl radical generation. Moreover, as the concentration of RhB increases, photons are intercepted before reaching the catalyst surface, resulting in reduced photon

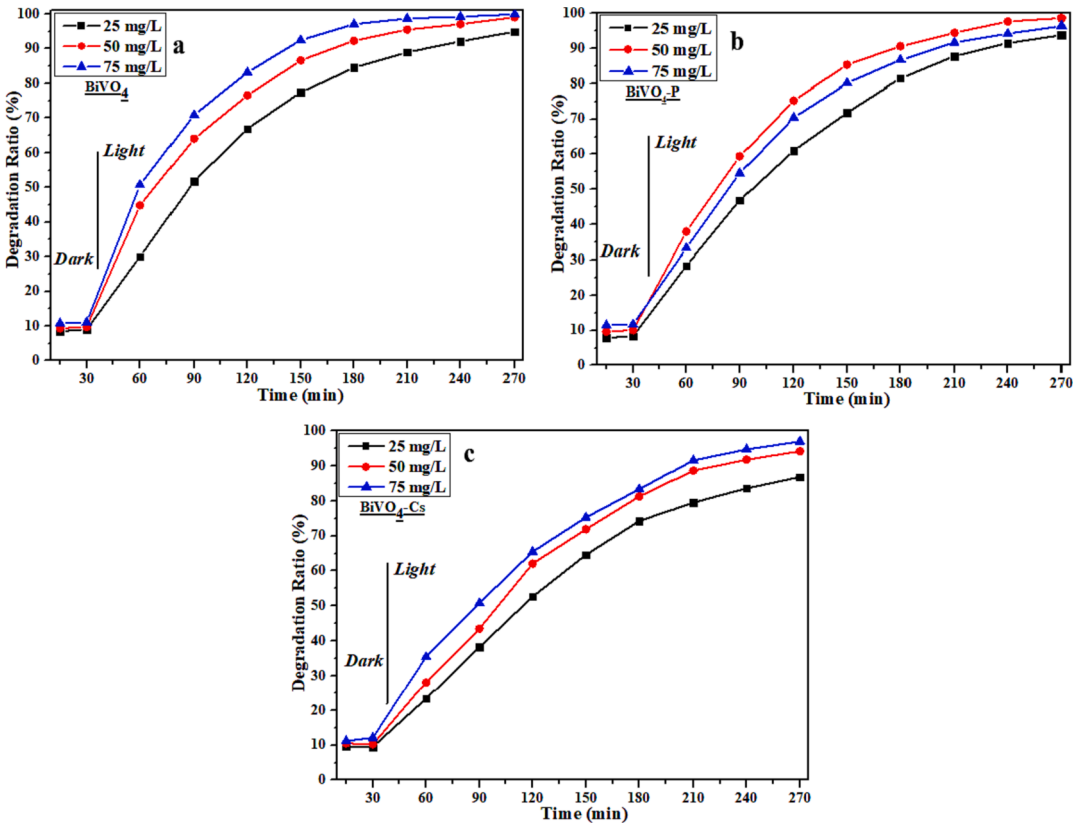

Fig. 8. Effect of the photocatalysts $BiVO_4$ (a), $BiVO_4$-P (b), and $BiVO_4$-Cs (c) dose on RhB degradation rate.

absorption by the catalyst and consequently diminishing RhB photodegradation rate [52].

The alteration of spectral properties during RhB degradation on $BiVO_4$-Cs was described in **Fig. S2**. A hypsochromic peak shift around 500 nm was observed, indicating the presence of an intermediate. Simultaneously, a reduction in absorbance intensity at the 554 nm peak was noted over the irradiation period with UV-B light, and no discernible shift towards lower wavelengths was observed. This pattern implies a degradation pathway characterized by chromophore cleavage, hydroxylation, aromatic ring opening, and ultimately, a mineralization process. The disruption of the conjugated structure in the degradation intermediates may lead to the formation of compounds such as carboxylic acids, dicarboxylic acids, amines, or other substances that neither absorb in the visible region nor exhibit additional absorption peaks in the 400–650 nm range [53].

3.2.4. Photocatalysts reusability

The photocatalyst was reused under the optimum conditions determined over five consecutive cycles. Catalysts were washed with DI water and dried at 100 °C at the end of each stage of the catalytic degradation process. The results showed (Fig. 10**a**) that the efficiency of the photocatalyst decreased as the number of regeneration steps increased. $BiVO_4$-Cs and $BiVO_4$-P were comparatively more stable than $BiVO_4$. The reduction in efficiency of the photocatalytic process could be due to damage and alteration of the catalytically active sites, reduction of the active surface area and pores in the catalyst structure.

3.2.5. Scavengers effect

Using the $BiVO_4$-Cs catalyst, a quenching experiment to identify the reactive species responsible for degrading the traps when exposed to visible light was carried out (Fig. 10**b**). In line with previous research, we have introduced the primary reactive species into each experimental solution as follows: EDTA (to trap h^+ holes), isopropanol (to trap ·OH radicals) and Na_2CO_3 (to trap $\cdot O^{2-}$ radicals). The photocatalyst was introduced after RhB solution was reacted with the scavengers. The effect of the scavengers on $BiVO_4$-Cs in the presence of RhB solution led to a reduction in removal efficiency, with Na_2CO_3 (74.47 %) > EDTA (58.09 %) > isopropanol (39.21 %). Thus, it appears that the effect of photocatalysis on RhB decomposition by the $\cdot O^{2-}$ trap was more pronounced when exposed to UV-B light compared to exposure to the h^+ and ·OH traps.

3.2.6. RhB photodegradation mechanism

As commonly acknowledged, the crucial characteristic of semiconducting materials is the value of the band gap energy. This property governs the route taken by charge carriers as they move, influencing the efficiency of photodegradation for organic pollutants. Eqs. (5) and (6) can be employed to ascertain the charge transport mechanism by analyzing the band edge positions of the sample.

$$E_{CB} = \chi - E_e - 0.5*E_g \tag{5}$$

$$E_{VB} = E_{CB} + E_g \tag{6}$$

Where E_g denotes the band gap energy, E_{VB} represents the valence band edge potential, and E_{CB} signifies the conduction band edge potential. The standard free electron energy on the hydrogen scale is denoted by E_e (~4.5 eV) [54]. The electronegativity of semiconductors, denoted as χ, can be computed using Eq. (7) [55]:

$$\chi\left(A_a B_b C_c\right) = \left(\chi(A)^a * \chi(B)^b * \chi(C)^c\right)^{\frac{1}{a+b+c}} \tag{7}$$

The coefficients a, b and c signify the number of atoms present in each composition. The electronegativity value for $BiVO_4$-Cs was determined to be 6.16 eV. The positions of the conduction band (CB) and valence band (VB) in this oxide were established at 0.37 and 2.95 eV, respectively. As a result, the catalyst can interact with O_2 to produce the $OH^{\bullet}$

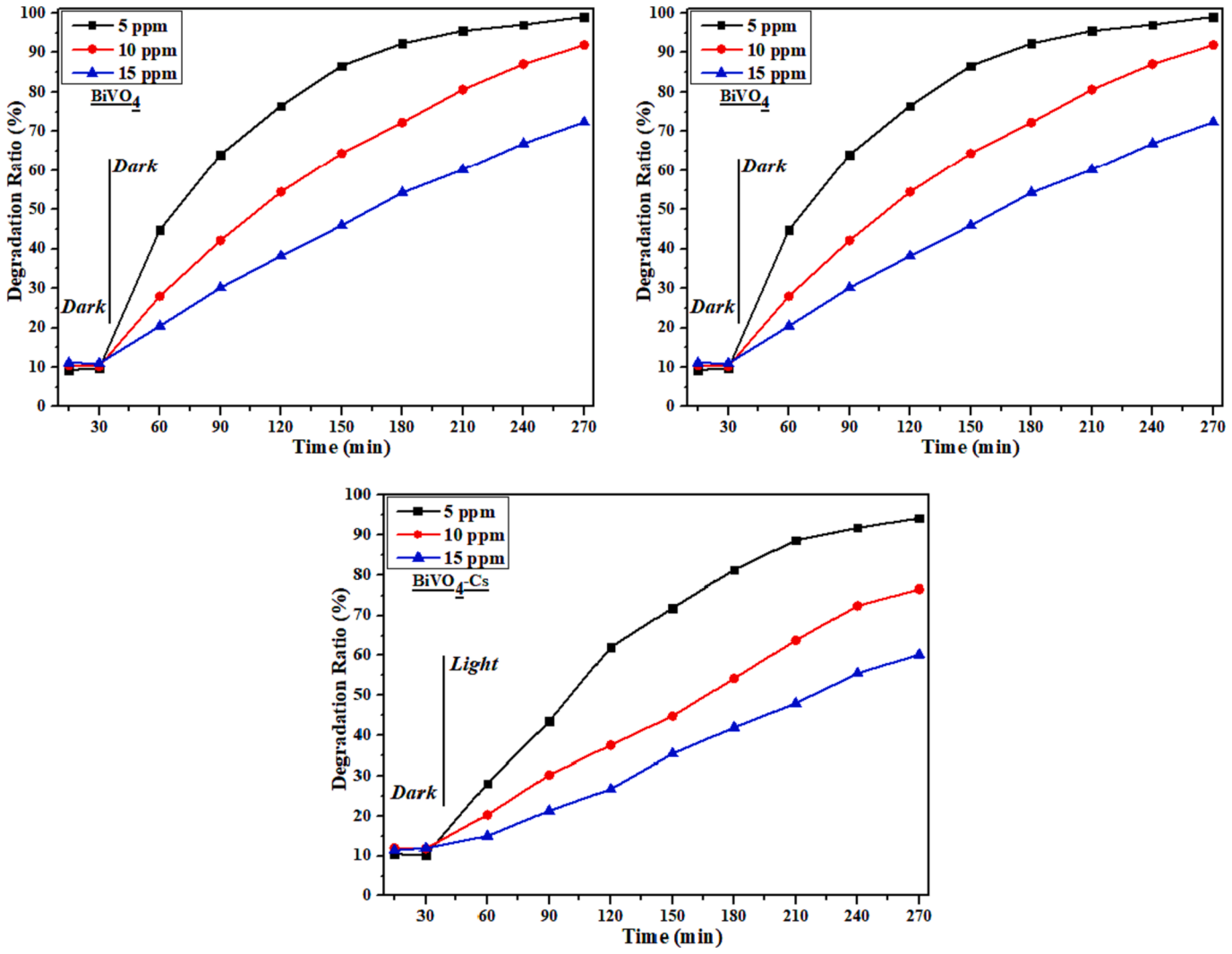

Fig. 9. Effect of the initial concentration on RhB photodegradation rate by $BiVO_4$ (a), $BiVO_4$-P (b), and $BiVO_4$-Cs (c).

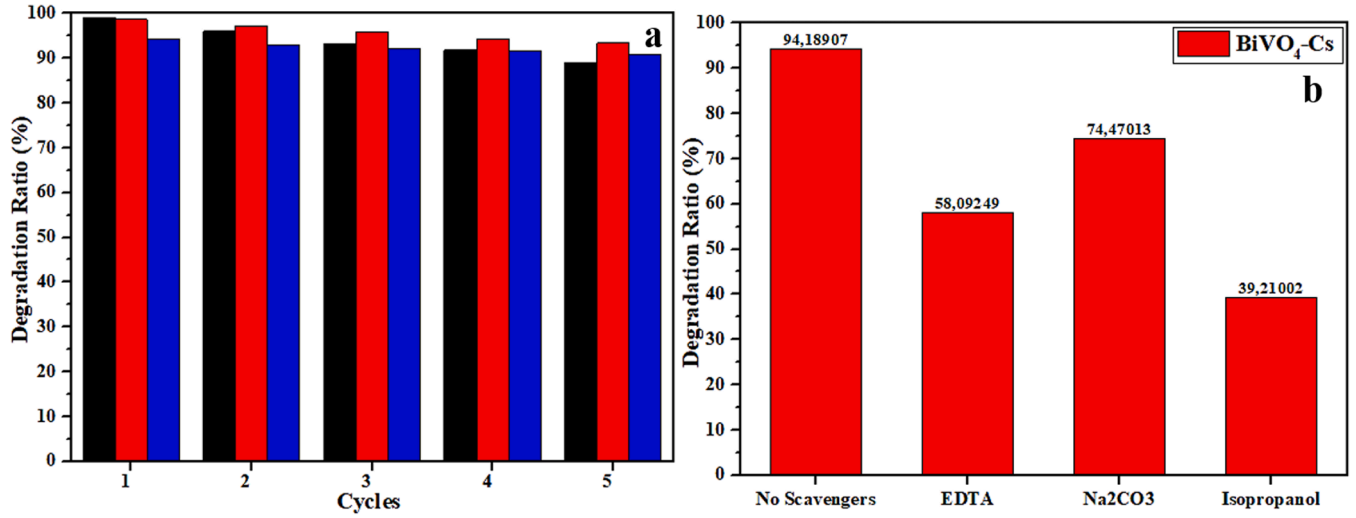

Fig. 10. Reusability plot for RhB photodegradation on samples (Black: $BiVO_4$, Red: $BiVO_4$-P, and Blue: $BiVO_4$-Cs) (a), and Plot displayed scavenging effect on RhB photodegradation in presence of $BiVO_4$-Cs for t: 240 min (b).

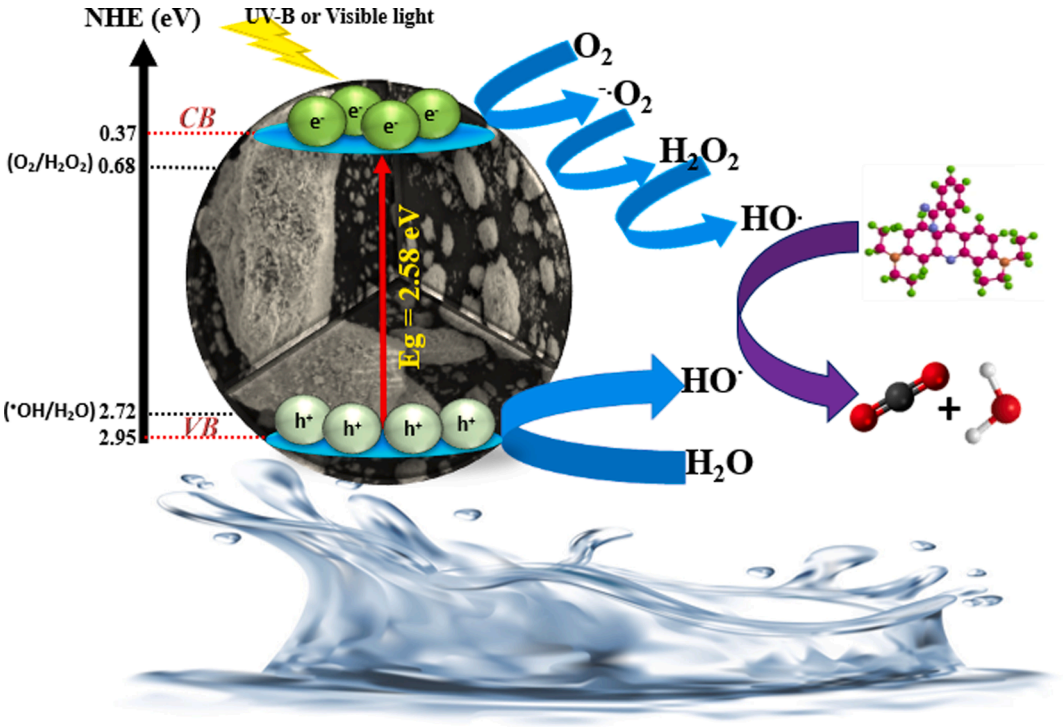

Fig. 11. Proposed mechanism of RhB photodegradation.

radical species through the reduction of O_2 to H_2O_2, followed by the further reduction of H_2O_2 to OH^- and the $OH^\bullet$ species. This capability stems from the lower CB edge potential of $BiVO_4$-Cs (E_{CB} = 0.37 eV / NHE) compared to the standard potential of the O_2/H_2O_2 redox couple (0.68 eV). Furthermore, the VB potential of $BiVO_4$ is 2.95 eV, higher than the standard redox potential of $^\bullet OH/H_2O$ (2.72 eV). As a result, adsorbed H_2O molecules can be oxidized to $^\bullet OH$ by the photogenerated h^+ in the VB. From Fig. 10b, it is evident that $^\bullet OH$ and h^+ have a great effect on the degradation of the RhB solution.

Fig. 11 illustrates a potential mechanism for the photocatalytic oxidation of RhB using $BiVO_4$ when exposed to UV-B light irradiation. The RhB degradation was a multi-step process, described through Eqs. (8) to (16).

During the initial step (Step 1, Eq. (8), the $BiVO_4$ catalyst absorbs irradiation and generates electron-hole pairs.

$$BiVO_4 + h\nu \rightarrow e^-(CB) + h^+(VB) \quad (8)$$

Step 2 involves the separation of charge carriers in the presence of water, resulting in the formation of superoxide anion radicals and hydroxyl radicals.

$$e^-(CB) + O_2 \rightarrow O_2^{\bullet -} \quad (9)$$

$$O_2^{\bullet -} + H^+ \rightarrow HO_2^\bullet \quad (10)$$

$$HO_2^\bullet + e^- \rightarrow HO_2^- \quad (11)$$

$$HO_2^- + H^+ \rightarrow H_2O_2 \quad (12)$$

$$H_2O_2 + e^- \rightarrow OH^\bullet + OH^- \quad (13)$$

$$h^+(VB) + H_2O \rightarrow OH^\bullet + H^+ \quad (14)$$

$$h^+(VB) + OH^- \rightarrow OH^\bullet \quad (15)$$

$$RhB + OH^\bullet \rightarrow \text{degradation by} - \text{product} \quad (16)$$

Table 1
RhB photocatalytic degradation rate constants of pseudo-first and pseudo-second order as well as their correlation coefficients.

Catalyst	UV-B light			
	K_1 (1/min)	R_1^2	K_2 (L/mg-min)	R_2^2
$BiVO_4$	0.01782	0.9874	0.0483	0.6271
$BiVO_4$-P	0.01769	0.9929	0.0406	0.7355
$BiVO_4$-Cs	0.01238	0.9849	0.0113	0.8727

3.2.7. Kinetic study

To further improve the understanding of RhB photocatalytic degradation using $BiVO_4$, $BiVO_4$-P and $BiVO_4$-Cs, the analysis of their kinetic behavior during the process has been conducted by applying pseudo-first order and pseudo-second order kinetic models, as shown in the following Eqs. (17) and (18).

$$\ln\left(\frac{C_0}{C_t}\right) = K_1 * t \quad (17)$$

$$\frac{1}{C_t} - \frac{1}{C_0} = K_2 * t \quad (18)$$

where C_0 and C_t are the RhB concentrations at initial and at any time t, K_1 and K_2 are the observed rate coefficients for the pseudo first-order and second-order reactions, respectively.

Fig. S3 displayed the plots of ln (C_0/C_t) and ($1/C_t - 1/C_0$) versus time (t) for the decomposition of RhB by $BiVO_4$, $BiVO_4$-P, and $BiVO_4$-Cs. From these plots, the rate constants and the correlation coefficients were calculated and reported in Table 1. Following the results of the study, a pseudo first-order model was found to be the most suitable model for effectively describing photocatalytic reactions involving all catalysts under UV-B light. Furthermore, the findings indicated that the rate constant (K_1) values for the $BiVO_4$ and $BiVO_4$-P catalysts were the highest, suggesting that photocatalytic reactions with these two photocatalysts occurred at considerably faster rate.

Table 2
Comparison of templates efficiency of some of the reported $BiVO_4$.

Synthesis method	Experimental conditions	Gap energy (eV)	SSA (m^2/g)	Photocatalytic activity	Reference
Hydrothermal	[$BiVO_4$] = 0.2 g/L; [RhB] = 1.5 ppm; irradiation time = 180 min	2.36	53.6	100% under Visible light	[57]
Co-precipitation	[$BiVO_4$] = 1g/L; [RhB] = 5 ppm; pH=10; irradiation time = 300 min	2.27	1.5	99 % under Visible light	[58]
Hydrothermal	[$BiVO_4$] = 1g/L; [RhB] = 15 ppm; irradiation time = 200 min	2.42	–	62.38% under Visible light	[59]
Solvothermal	[$BiVO_4$] = 2g/L; [RhB] = 8.6 ppm; irradiation time = 120 min	2.31	12.08	74.8 % under Visible light	[60]
Hydrothermal	[$BiVO_4$] = 1g/L; [RhB] = 20 ppm; irradiation time = 50 min	2.42	84.23	0.97 % under UV light	[61]
Hydrothermal	[$BiVO_4$] = 1g/L; [RhB] = 10 ppm; irradiation time = 240 min	($BiVO_4$-PVP) - 2.42	1.60	36.4 %	[38]
		($BiVO_4$-CTAB) - 2.41	2.90	94.9 %	
		($BiVO_4$-SDBS) - 2.45	3.90	89.4 % under Visible light	
Hydrothermal	[$BiVO_4$] = 1g/L; [RhB] = 5 ppm; pH = 7; irradiation time = 210 min	($BiVO_4$) – 2.61	9.20	99.04 % under UV-B light 82.10 % under Visible light	This Work
		($BiVO_4$-P) – 2.56	11.59	98.61 % under UV-B light 76.11 % under Visible light	
		($BiVO_4$-Cs) – 2.58	12.27	94.18 % under UV-B light 64.40 % under Visible light	

3.2.8. *Visible light investigation*

Using the optimal conditions determined from the preceding study, we have tested the photocatalytic activity of the photocatalysts under visible light irradiation. The results presented in **Fig. S4** indicate that all catalysts exhibited photocatalytic activity upon exposure to visible light, albeit to a lesser extent compared to UV-B light. The observed RhB degradation rates for $BiVO_4$, $BiVO_4$-P, and $BiVO_4$-Cs in 270 min were 82, 76, and 67 %, respectively. These results suggest that their photocatalytic activity is not particularly strong, which could be attributed to various factors, including the synthesis method and directing agents used. These factors directly influenced the particle morphology and the photocatalytic efficiency of the catalysts[36,56].

3.2.9. *Performance comparison*

Table 2 [36,37,54–57] presented a detailed performance comparison between synthesized $BiVO_4$ catalysts, which were meticulously prepared using the hydrothermal method, and a range of other $BiVO_4$ catalysts synthesized with various directing agents. The data clearly illustrates that the catalysts developed during current study exhibits highly promising results, demonstrating a remarkable level of efficiency in their performance. This suggests that reported hydrothermal synthesis method had yielded catalysts that outperform their counterparts synthesized with different directing agents.

4. Conclusions

In this research, $BiVO_4$ photocatalyst was successfully synthesized through hydrothermal method, with the utilization of two different templating agents: Cs as an ecological an economical template and P as a surfactant. The SEM and TEM analyses revealed that the choice of templating agent significantly influenced the morphology and size of these photocatalysts. Interestingly, when templates were not used, formation of irregularly shaped clusters with large sizes was observed. However, the introduction of directing agents resulted in the creation of smaller irregular shapes, especially when Cs was employed. N_2 adsorption indicated an increase in the specific surface area from 9.20 to 12.27 m^2/g when employing Cs as a model. The XPS analysis demonstrated that the templates significantly influence the material's surface charge, as evidenced by the examination of pH_{PZC}. These synthesized samples were subsequently employed as photocatalysts to degrade RhB under UV-B and visible light exposure. Photocatalysts created with the aid of templates exhibited remarkable catalytic stability, but they displayed lower photocatalytic performance in removing the targeted pollutant, despite having the highest SSA. In addition, $BiVO_4$ synthesized without the use of templates exhibited higher degradation rate following a pseudo first order reaction compared to the samples synthesized with templating agents. The application of Cs during the synthesis of $BiVO_4$ seems promising, as it gives notable results in terms of photodegradation. Nevertheless, improvements in $BiVO_4$-Cs synthesis conditions are needed to maximize its photodegradation efficiency.

CRediT authorship contribution statement

Said Essenni: Writing – original draft, Investigation, Formal analysis, Data curation. **Moonis Ali Khan:** Writing – review & editing, Software, Resources. **Rachid El kaim billah:** Project administration, Investigation, Conceptualization. **Byong-Hun Jeon:** Writing – review & editing. **Suresh Sundaramurthy:** Writing – review & editing. **Mahfoud Agunaou:** Writing – review & editing, Supervision, Conceptualization.

Declaration of competing interest

The authors declare that they have no known competing financial interests or personal relationships that could have appeared to influence the work reported in this paper.

Data availability

Data will be made available on request.

Acknowledgments

Moonis Ali Khan acknowledges the financial support through Researchers Supporting Project number (RSP2024R345), King Saud University, Riyadh. Saudi Arabia

Appendix A. Supplementary material

Supplementary data to this article can be found online at https://doi.org/10.1016/j.molliq.2024.124270.

References

[1] M.B.K. Kader, S. Al-Mamun, M.R. Suhan, M.S. Shuchi, S.B. Islam, Enhanced photodegradation of methyl orange dye under UV irradiation using MoO_3 and Ag doped TiO_2 photocatalysts, Environ. Technol. Innov. 27 (2022) 102476.

[2] A. Esrafili, M. Salimi, A.J. Jafari, H.R. Sobhi, M. Gholami, R.R. Kalantary, Pt-based TiO_2 photocatalytic systems: a systematic review, J. Mol. Liq. 352 (2022) 118685.

[3] Z. Li, S. Wang, J. Wu, W. Zhou, Recent progress in defective TiO_2 photocatalysts for energy and environmental applications, Renew. Sustain. Energy Rev. 156 (2022) 111980.

[4] A.S.M. Nur, M. Sultana, A. Mondal, S. Islam, F.N. Robel, A. Islam, M.S.A. Sumi, A review on the development of elemental and codoped TiO_2 photocatalysts for enhanced dye degradation under UV–VIS irradiation, J. Water Process Eng. 47 (2022) 102728.

[5] T. Sansenya, N. Masri, T. Chankhanittha, T. Senasu, J. Piriyanon, S. Mukdasai, S. Nanan, Hydrothermal synthesis of ZnO photocatalyst for detoxification of anionic azo dyes and antibiotic, J. Phys. Chem. Solids 160 (2022) (2022) 110353.

[6] T. Kanagaraj, P.S.M. Kumar, R. Thomas, R. Kulandaivelu, R. Subramani, R. N. Mohamed, S. Lee, S.W. Chang, W.J. Chung, D.D. Nguyen, Novel pure α-, β-, and mixed-phase α/β-Bi_2O_3 photocatalysts for enhanced organic dye degradation under both visible light and solar irradiation, Environ. Res. 205 (2022) (2022) 112439.

[7] M.R. Al-Mamun, S. Kader, M.S. Islam, M.Z.H. Khan, Photocatalytic activity improvement and application of UV-TiO_2 photocatalysis in textile wastewater treatment: a review, J. Environ. Chem. Eng. 7 (5) (2019) 103248.

[8] Y. Park, K.J. Mc Donald, K.-S. Choi, Progress in bismuth vanadate photoanodes for use in solar water oxidation, Chem. Soc. Rev. 42 (6) (2013) 2321–2337.

[9] A. Zhang, J. Zhang, Characterization of visible-light-driven $BiVO_4$ photocatalysts synthesized via a surfactant-assisted hydrothermal method, spectrochim. acta - part a Mol, Biomol. Spectrosc. 73 (2) (2009) 336–341.

[10] M. Zalfani, M. Mahdouani, R. Bourguiga, B.L. Su, Experimental and theoretical study of optical properties and quantum size phenomena in the $BiVO_4/TiO_2$ nanostructures, Superlatt. Microstruct. 83 (2015) 730–744.

[11] S. Tokunaga, H. Kato, A. Kudo, Selective preparation of monoclinic and tetragonal $BiVO_4$ with scheelite structure and their photocatalytic properties, Chem Mater. 13 (12) (2001) 4624–4628.

[12] X. Zhang, Z. Ai, F. Jia, L. Zhang, X. Fan, Z. Zou, Selective synthesis and visible-light photocatalytic activities of $BiVO_4$ with different crystalline phases, Mater. Chem. Phy. 103 (2007) 162–167.

[13] A. Kudo, K. Omori, H. Kato, A novel aqueous process for preparation of crystal form-controlled and highly crystalline $BiVO_4$ powder from layered vanadates at room temperature and its photocatalytic and photophysical properties, J. Am. Chem. Soc. 121 (1999) 11459–11467.

[14] S. Kohtani, S. Makino, A. Kudo, K. Tokumura, Y. Ishigaki, T. Matsunaga, O. Nikaido, K. Hayakawa, R. Nakagaki, Photocatalytic degradation of 4-n-nonylphenol under irradiation from solar simulator : comparison between BiVO4 and TiO2 photocatalysts, Chem. Lett. 7 (2002) 660–661.

[15] B. Xie, H. Zhang, P. Cai, R. Qiu, Y. Xiong, Simultaneous photocatalytic reduction of cr (VI) and oxidation of phenol over monoclinic BiVO4 under visible light irradiation, Chemosphere 63 (2006) 956–963.

[16] Y. Zou, M. Lu, Z. Jiang, L. Xu, C. Liu, L. Zhang, Y. Chen, Hydrothermal synthesis of zn-doped $BiVO_4$ with mixed crystal phase for enhanced photocatalytic activity, Opt. Mater. 119 (2021) 111398.

[17] Y. Lin, C. Lu, C. Wei, Microstructure and photocatalytic performance of $BiVO_4$ prepared by hydrothermal method, J. Alloys Compd. 781 (2019) (2019) 56–63.

[18] B.-X. Lei, L.L. Zeng, P. Zhang, Z.-F. Sun, W. Sun, X.-X. Zhang, Hydrothermal synthesis and photocatalytic properties of visible-light induced $BiVO_4$ with different morphologies, Adv. Powder Technol. 25 (3) (2014) 946–951.

[19] J.P. Deebasree, V. Maheskumar, B. Vidhya, Investigation on the impact of pH on the photocatalytic activity of sonochemically synthesised $BiVO_4$, Mater. Lett. 311 (2022) 131571.

[20] J.P. Deebasree, V. Maheskumar, B. Vidhya, Investigation on the structural and optical properties of sonochemically synthesized - $BiVO_4$ for photocatalytic degradation of methylene blue, J. Mater. Sci.: Mater. Electron. 29 (2018) 10715–10722.

[21] J.-S. Ma, L.-Y. Lin, Y.-S. Chen, Facile solid-state synthesis for producing molybdenum and tungsten co-doped monoclinic $BiVO_4$ as the photocatalyst for photoelectrochemical water oxidation, Int. J. Hydrogen Energy 44 (16) (2019, 2019,) 7905–7914.

[22] W. Yin, W. Wang, L. Zhou, S. Sun, L. Zhang, CTAB-assisted synthesis of monoclinic $BiVO_4$ photocatalyst and its highly efficient degradation of organic dye under visible-light irradiation, J Hazard. Mater. 173 (1–3) (2010) 194–199.

[23] U.M.G. Pérez, S. Sepúlveda-Guzmán, A. Martínez-de la Cruz, U.O. Méndez, Photocatalytic activity of $BiVO_4$ nanospheres obtained by solution combustion synthesis using sodium carboxymethylcellulose, J. Mol. Cataly. A : Chem. 335 (2011) 169–175.

[24] W. Sun, M. Xie, L. Jing, Y. Luan, H. Fu, Synthesis of large surface area nano-sized $BiVO_4$ by an EDTA-modified hydrothermal process and its enhanced visible photocatalytic activity, J. Solid State Chem. 184 (11) (2011) 3050–3054.

[25] X. Meng, L. Zhang, H. Dai, Z. Zhao, R. Zhang, Y. Liu, Surfactant-assisted hydrothermal fabrication and visible-light-driven photocatalytic degradation of methylene blue over multiple morphological BiVO4 single-crystallites, Mater. Chem. Phys. 125 (1–2) (2011) 59–65.

[26] H. Jiang, X. Meng, H. Dai, J. Deng, Y. Liu, L. Zhang, Z. Zhao, R. Zhang, High-performance porous spherical or octapod-like single-crystalline $BiVO_4$ photocatalysts for the removal of phenol and methylene blue under visible-light illumination, J. Hazard. Mater. 217–218 (2012) 92–99.

[27] Z. Wu, Y. Xue, X. He, Y. Li, X. Yang, Z. Wu, G. Cravotto, Surfactants-assisted preparation of $BiVO_4$ with novel morphologies via microwave method and CdS decoration for enhanced photocatalytic properties, J. Hazard. Mater. 387 (2020) 122019.

[28] S. Obregón, A. Caballero, G. Colón, Hydrothermal synthesis of $BiVO_4$: structural and morphological influence on the photocatalytic activity, Appl. Catal. B Environ. 117–118 (2012) 59–66.

[29] C. Regmi, D. Dhakal, S.W. Lee, Visible-light-induced Ag/$BiVO_4$ semiconductor with enhanced photocatalytic and antibacterial performance, Nanotechnology 29 (6) (2018) 064001.

[30] S. Pookmanee, Pusit kojinok, suchanya phanichphant, photocatalytic degradation of 2,4-dichlorophenol using $BiVO_4$ powder prepared by the sol–gel method, Trans. Mater. Res. Soc. Japan 39 (4) (2014) 431–434.

[31] D. Zhou, L.X. Pang, J. Guo, H. Wang, X. Yao, C. Randall, Phase evolution, phase transition, raman spectra, infrared spectra, and microwave dielectric properties of low temperature firing (K 0.5xBi1-0.5x)(MoxV1-x)O4 ceramics with scheelite related structure, Inorg. Chem. 50 (24) (2011) 12733–12738.

[32] M.M. Sajid, S.B. Khan, Y. Javed, N. Amin, N.A. Shad, Z. Zhang, H. Zhai, Facile synthesis of Se/$BiVO_4$ heterojunction composite and evaluation of synergetic reaction mechanism for efficient photocatalytic staining of organic dye pollutants in wastewater under visible light, J. Mater. Sci. Mater. Electron. 31 (2020) (2020) 19599–19612.

[33] S.D. Abraham, S.T. David, R.B. Bennie, C. Joel, D.S. Kumar, Eco-friendly and green synthesis of $BiVO_4$ nanoparticle using microwave irradiation as photocatalayst for the degradation of alizarin red S, J. Mol. Struct. 1113 (2016) 174–181.

[34] M.A. Butler, Photoelectrolysis and physical properties of the semiconducting electrode WO_2, J. Appl. Phys. 48 (1977) 1914–1920.

[35] L. Zhou, W. Wang, S. Liu, L. Zhang, H. Xu, W. Zhu, A sonochemical route to visible-light-driven high-activity $BiVO_4$ photocatalyst, J. Mol. Catal. A Chem. 252 (1–2) (2006) 120–124.

[36] H. Fan, D. Wang, L. Wang, H. Li, P. Wang, T. Jiang, T. Xie, Hydrothermal synthesis and photoelectric properties of $BiVO_4$ with different morphologies: an efficient visible-light photocatalyst, Appl. Surf. Sci. 257 (17) (2011) 7758–7762.

[37] J. Zeng, J. Zhong, J. Li, Z. Xiang, X. Liu, J. Chen, Improvement of photocatalytic activity under solar light of $BiVO_4$ microcrystals synthesized by surfactant-assisted hydrothermal method, Mater. Sci. Semicond. Process. 27 (2014) 41–46.

[38] J. Liu, B. Li, L. Kong, Q. Xiao, S. Huang, Surfactants-assisted morphological regulation of $BiVO_4$ nanostructures for photocatalytic degradation of organic pollutants in wastewater, J. Phys. Chem. Solids 172 (2023) 111079.

[39] H. Jalili, B. Aslibeiki, A.G. Varzaneh, V.A. Chernenko, The effect of magneto-crystalline anisotropy on the properties of hard and soft magnetic ferrite nanoparticles, Beilstein J. Nanotechnol. 10 (2019) 1348–1359.

[40] S. Irfan, Y. Shen, S. Rizwan, H.-C. Wang, S.B. Khan, C.-W. Nan, Band-gap engineering and enhanced photocatalytic activity of sm and mn doped $BiFeO_3$ nanoparticles, J. Am. Ceram. Soc. 100 (1) (2017) 31–40.

[41] S. Fatima, S.I. Ali, M.Z. Iqbal, S. Rizwan, The high photocatalytic activity and reduced band gap energy of la and mn co-doped BiFeO3/graphene nanoplatelet (GNP) nanohybrids, RSC Adv. 7 (57) (2017) 35928–35937.

[42] M.M. Sajid, S.B. Khan, N.A. Shad, N. Amin, Synthesis of Zn3(VO4)2/BiVO4 heterojunction composite for the photocatalytic degradation of methylene blue organic dye and electrochemical detection of H2O2, RSC Adv. 8 (62) (2018) 35403–35412.

[43] H. Bai, P. Guan, K. Qu, W. Fan, F. Wang, D. Xu, J. Ding, W. Shi, Reasonable regulation of kinetics over $BiVO_4$ photoanode by Fe–CoP catalysts for boosting photoelectrochemical water splitting, Int. J. Hydrogen Energy 44 (52) (2019) 28184–28193.

[44] S. Bai, Q. Li, J. Han, X. Yang, X. Shu, J. Sun, L. Sun, R. Luo, D. Li, A. Chen, Photoanode of LDH catalyst decorated semiconductor heterojunction of $BiVO_4$/CdS to enhance PEC water splitting efficiency, Int. J. Hydrogen Energy 44 (45) (2019) 24642–24652.

[45] S. Wang, P. Chen, Y. Bai, J.-H. Yun, G. Liu, L. Wang, New $BiVO_4$ dual photoanodes with enriched oxygen vacancies for efficient solar-driven water splitting, Adv. Mater. 30 (2018) 1800486.

[46] L.H. Dall'Antonia, N.R. de Tacconi, W. Chanmanee, H. Timmaji, N. Myung, K. Rajeshwar, Electrosynthesis of bismuth vanadate photoelectrodes, Electrochem. Solid-State Lett. 13 (5) (2010) 29–32.

[47] J.-M. Wu, Y. Chen, L. Pan, P. Wang, Y. Cui, D.C. Kong, L. Wang, X. Zhang, J.-J. Zou, Multi-layer monoclinic BiVO4 with oxygen vacancies and V4+ species for highly efficient visible-light photoelectrochemical applications, Appl. Catal. B Environ. 221 (2018) 187–195.

[48] Q.A.H. Al-Naser, J. Zhou, H. Wang, G. Liu, L. Wang, Synthesis and optical properties of MgO-doped ZnO microtubes using microwave heating, Opt. Mater. 46 (2015) 22–27.

[49] K. Ravichandran, N.S. Jyothi, K. Thirumurugan, S. Suvathi, N. Chidhambaram, R. Uma, B. Sundaresan, Influence of Mo+F incorporation and point of zero charge on the dye degradation efficacy of ZnO thin films, Chem. Phys. 564 (2023) 111714.

[50] M.M. Khalaf, E. Da'na, K. Al-Amer, M. Hessien, Experimental design modeling of the effect of hexagonal wurtzite-ZnO synthesis conditions on its characteristics and performance as a cationic and anionic adsorbent, Molecules 24 (21) (2019) 3884.

[51] G. Fan, R. Ning, Z. Yan, J. Luo, B. Du, J.L. Liu, J. Zhang, Double photoelectron-transfer mechanism in Ag−AgCl/WO_3/g-C_3N_4 photocatalyst with enhanced visible-light photocatalytic activity for trimethoprim degradation, J. Hazard. Mater. 403 (2021) 123964.

[52] G. Fan, S. Yang, B. Du, J. Luo, X. Lin, X. Li, Sono-photo hybrid process for the synergistic degradation of levofloxacin by $FeVO_4$/$BiVO_4$: mechanisms and kinetics, Environ. Res. 204 (2022) 112032.

[53] L. Liang, L. Cheng, Y. Zhang, Q. Wang, Q. Wu, Y. Xue, X. Meng, Efficiency and mechanisms of rhodamine B degradation in Fenton-like systems based on zero-valent iron, RSC Adv. 48 (2020) 28509–28515.
[54] M. Abdi, V. Mahdikhah, S. Sheibani, Visible light photocatalytic performance of La-Fe co-doped $SrTiO_3$ perovskite powder, Opt. Mater. 102 (2020) (2020) 109803.
[55] Z. Chchiyai, L. Hdidou, M. Tayoury, A. Chari, Y. Tamraoui, J. Alami, M. Dahbi, B. Manoun, Synthesis and electrochemical properties of mn-doped porous Mg0.9Zn0.1Fe2−xMnxO4 ($0 \leq x \leq 1.25$) spinel oxides as anode materials for lithium-ion batteries, J. Alloys Compd. 935 (2023) 167997.
[56] S. Dong, J. Feng, Y. Li, L. Hu, M. Liu, Y. Wang, Y. Pi, J. Sun, J. Sun, Shape-controlled synthesis of $BiVO_4$ hierarchical structures with unique natural-sunlight-driven photocatalytic activity, Appl. Catal. B Environ. 152–153 (2014) 413–424.
[57] X. Lin, H. Li, L. Yu, H. Zhao, Y. Yan, C. Liu, H. Zhai, Efficient removal rhodamine B over hydrothermally synthesized fishbone like $BiVO_4$, Mater. Res. Bull. 48 (10) (2013) 4424–4429.
[58] A. Martínez-de la Cruz, U.M. Gracia Pérez, Photocatalytic properties of $BiVO_4$ prepared by the co-precipitation method: degradation of rhodamine B and possible reaction mechanisms under visible irradiation, Mater. Res. Bull. 45 (2) (2010) 135–141.
[59] N.D. Trinh, H. Hoang, N.X. Linh, N.H. Vinh, H.T. Vu, H.T. Nguyen, S. Do, D.v., N-vo, visible light induced enhanced photocatalytic degradation of industrial effluents (rhodamine B) using BiVO4 nanoparticles, IOP conf. ser, Mater. Sci. Eng. 542 (2019) n.pag, https://doi.org/10.1088/1757-899X/542/1/012060.
[60] L. Ma, L.-M. Xu, L.-L. Zhang, Hierarchical $BiVO_4$ micro/nanostructures synthesised via a solvothermal route and photodegradation of rhodamine B, micro, Nano Lett. 9 (7) (2014, 2014,) 451–454.
[61] K. Liu, X. Shen, H. Shen, K. Jiang, T. Sun, M. Wang, One-step fabrication of novel $BiVO_4$ hollow nanotubes with improved photocatalytic activity, Mater. Lett. 349 (2023) 134792.